

ULF power fluctuations in the solar-wind parameters and their relationship with the relativistic electron flux at the geosynchronous orbit

M. REGI^(*)

Dipartimento di Scienze Fisiche e Chimiche, Università degli Studi dell'Aquila - L'Aquila, Italy

received 29 January 2016

Summary. — We focused the attention on the Pc5 geomagnetic pulsations in response to the solar wind forcing and their relationship with the relativistic electron flux at geostationary orbit. We present here the results of a correlation analysis between the Pc5 power in the magnetosphere and on the ground, at low and high latitude, and the solar-wind speed and fluctuation power of the interplanetary magnetic field and solar-wind dynamic pressure through the years 2006 to 2010, also showing the relative timing between pulsations and solar-wind parameters. The Pc5 power appears significantly correlated with simultaneous solar-wind pressure fluctuations and with the solar-wind speed lagged by several hours. The relative amplitude of the two correlation peaks depends on the solar cycle phase and on the latitude. We also show a strong relationship between the Pc5 power and the > 600 keV and > 2 MeV electron flux at geosynchronous orbit. Clear evidence emerges that the electron flux follows the Pc5 power by about 2 days; the time delay is a bit longer for the higher-energy electrons.

1. – Introduction

The Earth, and the other planets of the solar system, are continuously invested by the full ionized gas escaping from the Sun atmosphere. The solar wind (SW), flowing outward from the Sun, exerts pressure upon interplanetary matter, evident for example from observations of comet tails [1]. The high conductivity of interplanetary plasma implies that the motion of matter couples to the deformation of the magnetic field so that the field lines follow the motion of matter. Alfvén called these field lines “frozen-in” [2]. It follows that the Earth’s magnetic field, originated in the inner core, is confined by the SW in a circumterrestrial region, also called magnetosphere (see [3] for an introduction).

^(*) E-mail: mauro.regi@aquila.infn.it

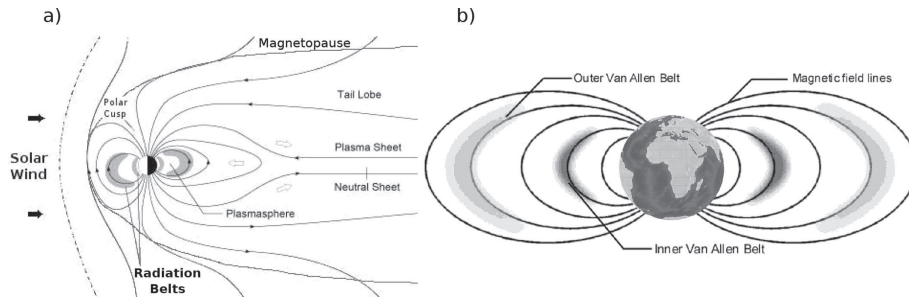


Fig. 1. – (a) Schematic representation of the Earth’s magnetosphere in the meridian plane (figure redrawn from <https://ase.tufts.edu/cosmos/>). In this figure the Sun is on the left side. (b) Schematic representation of the inner and outer Van Allen radiation belts (figure redrawn from <http://www.nasa.gov/>).

A sketch of the Earth’s magnetosphere is shown in fig. 1(a), together with its different regions, each characterized by different physical phenomena. We focused our attention on the radiation belts (fig. 1(b)).

The radiation (or Van Allen) belts were discovered in 1958 based on measurements from Geiger counters carried by the Explorer 1 spacecraft [4]. These regions comprise energetic charged particles trapped by the Earth’s magnetic field, with energies that range from keV to MeV. The inner belt region is located at $\sim 1.5\text{--}2$ Re (1 Re = 6380 km is the Earth’s radius) and it contains electrons, protons, and ions, while the outer belt region is located at $\sim 3\text{--}6$ Re and it contains essentially electrons.

Under adiabatic conditions, the energy of each trapped particle is conserved, and the Earth’s magnetic field guides the particle’s motion (fig. 2(a)). The trajectory of the guiding center, *i.e.* the instantaneous center of gyration orbit of a particle around the local magnetic field, can be divided into three distinct motions (see fig. 2(b)), since each of them is characterized by frequencies very different with respect to the others [5, 6].

Due to the Lorentz force the relativistic particle of mass at rest m_0 , velocity v and charge q , rotates around the local magnetic field B at the cyclotron frequency $f = qB/2\pi m_0\gamma$ (gyro motion), where $\gamma = (1 - (v/c)^2)^{-1/2}$ is the relativistic factor and c is the speed of light [6]. This represents the most rapid motion, and the resulting magnetic moment $M = p_{\perp}^2/2m_0B$ is conserved (first adiabatic invariant), where p_{\perp} is the component of the relativistic particle momentum \vec{p} perpendicular to the local magnetic field \vec{B} .

If the component of the relativistic particle moment p_{\parallel} parallel to the local magnetic field \vec{B} at the magnetic equator is not null, the particles move along the magnetic field line (fig. 2(a)). In this case, since the magnetic field intensifies when the particle approaches the magnetic footprints, and the energy is conserved, the direction of the motion is inverted before the particle precipitation: the particle travels back and forth between the northern and southern mirror points (bounce motion), and the quantity $J = \oint p_{\parallel} ds$ is also conserved (second adiabatic invariant), where s is the curvilinear distance of the magnetic field line from the equator to its footprint.

Finally, since the Earth’s magnetic field (approximated by a dipole field), intensifies radially earthward in the equatorial plane, the azimuthal drift motion of the guiding center occurs, and the magnetic flux Φ enclosed by the drift shell is conserved (third adiabatic invariant). Table I summarizes the particle motion and its associated adiabatic

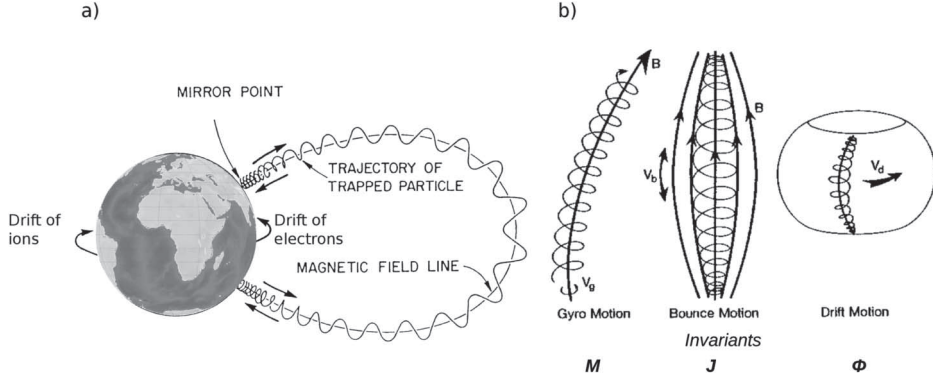


Fig. 2. – (a) Schematic representation of the guiding-center trajectory of a magnetically trapped charged particle in the magnetosphere (figure adapted from [7]). (b) Guiding-center motions (from left to right): gyro, bounce and drift motions associated with the first M , the second J , and the third Φ adiabatic invariants respectively (figure adapted from [3]). The gyro and drift motion pictures refer to electrons, while for ions the direction is opposite.

TABLE I. – *Characteristic time scales for the three types of trapped-particle motion.*

Motion	Invariant	Electron period [s]	Proton period [s]
Gyro	M	10^{-3} – 10^{-4}	10^{-1} – 10^{-2}
Bounce	J	10^{-1}	10^0
Drift	Φ	10^2 – 10^3	10^2

invariants, together with the characteristic periodicities for both protons and electrons (table from [8]).

2. – The dynamical interaction of the radiation belts with the ULF waves

While the inner belt is very stable, the outer belt exhibits a complex dynamic in response to SW and magnetospheric conditions, if the adiabatic condition is unsatisfied. It is now well established that disturbances in a magnetized plasma propagate as magnetohydrodynamic (MHD) waves, with frequencies that depend on their origin: in the SW or from processes within the magnetosphere [9]. Regarding the Ultra-Low-Frequency (ULF, 1 mHz to 5 Hz) waves, observed on the ground, they are divided into characteristic frequency ranges reported in table II.

TABLE II. – *Ultra-Low-Frequency wave classification associated with continuous pulsations.*

Pulsation type	Frequency range [mHz]	Period range [s]	Source location
Pc5	2–7	150–600	solar wind
Pc4	7–22	45–150	solar wind
Pc3	22–100	10–45	solar wind
Pc2	100–200	5–10	magnetosphere
Pc1	200–5000	0.2–5	magnetosphere

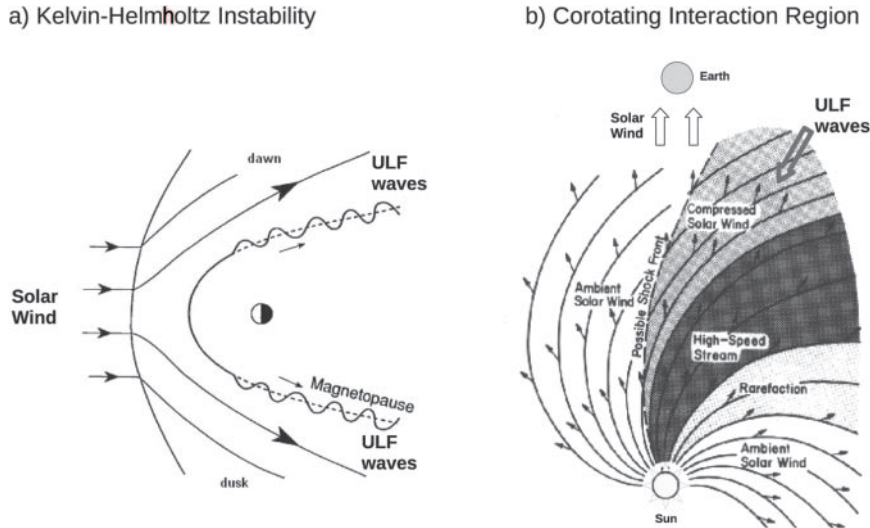


Fig. 3. – ULF waves generated across the magnetopause dawn/dusk flanks by Kelvin-Helmholtz Instability (left, adapted from [10]), and in the Corotating Interaction Region (right, adapted from [11]).

ULF fluctuations of the geomagnetic field have received in recent years considerable attention as they are involved in the acceleration of magnetospheric electrons in the radiation belts [9]. In this regard, several studies have shown that intense and persistent activity of ULF waves in the low-frequency range (1 to 7 mHz, Pc5 pulsations), observed at auroral latitudes, was followed within 1 to 2 days by enhanced fluxes of relativistic electrons (approximately MeV) at geosynchronous orbit [12-14].

Indeed, since the frequency of the Pc5 waves is comparable to the trapped-electron drift frequency (see table I and II), an acceleration can occur through resonant interaction of the ULF electric- and magnetic-field oscillations with the electron drift motion, leading to violation of the third adiabatic invariant and inward radial transport of accelerated electrons [6, 15, 16].

Experimental observations showed that ULF waves in the Pc5 frequency band are generally associated with processes described here and shown in fig. 3 (see also [9] for a review):

- The Kelvin-Helmholtz Instability (KHI), essentially developed on the magnetopause flanks, drives ULF waves, which propagate inward in the magnetosphere. During their inward propagation, the compressional waves transfer energy to the magnetosphere via coupling with transverse waves, due to the magnetospheric inhomogeneity (see for example [3] for a review). Such waves propagate along the magnetic field lines, and can be observed on the ground as Pc5, essentially at high latitudes (fig. 3(a)).
- Waves in the Pc5 frequency range are also observed in the interplanetary region between slow and fast SW streams, which are emanated by the Sun's corona [17]. Since the Sun's rotation period with respect to the Earth's reference system, is ~ 27 days, these regions are observed recurrently as Corotating Interaction Regions (CIR), and can impact on the magnetosphere transferring energy (fig. 3(b)).

Significant correlation was found between the SW speed and the Pc5 power, with a delay of approximately 1 day, *i.e.*, during the rising phase of fast SW speed streams ([18, 14]); such result, which appears somewhat inconsistent with the KHI driving mechanism (fig. 3(a)), has been explained by [18] still in terms of the KHI, pointing out that, in addition to the SW speed, the compression at the leading edge of fast SW streams could increase the growth rate of the instability.

3. – The SW-driven Pc5 power fluctuations

Recently, an analysis has been conducted [19] regarding the ULF waves power, in the Pc5 frequency band, simultaneously observed on the ground, at low (L’Aquila, AQU, $\lambda \sim 36^\circ\text{N}$) and high (Terra Nova bay, TNB, $\lambda \sim 80^\circ\text{S}$) geomagnetic latitude, and in the magnetosphere at geosynchronous orbit (GOES satellites, $L \sim 6.6$ Re).

Taking into account that the power P typically undergoes changes of several orders of magnitude between adjacent measurements, in the average procedure $\log P$ is used since it exhibits a quasi-normal distribution, instead of P . Figure 4 (adapted from [19]) shows the hourly values of SW speed V_{SW} , SW magnetic and pressure fluctuations power, and geomagnetic power, from March to April 2006. It clearly emerges that the V_{SW} maximum (marked by vertical dashed lines) follows the Pc5 power maximum of the geomagnetic field (Pc5_{AQU} and Pc5_{TNB}), SW pressure P_{nV^2} , and Interplanetary Magnetic-Field (IMF) fluctuation power P_B , mostly at time delays of several hours, consistently with the values also obtained by means of a cross-correlation analysis between SW speed and SW/IMF fluctuation power and geomagnetic field power.

Since high-latitude Pc5 power is stronger at the leading edge of SW streams, in contrast with the KHI as a driving process, using simulated SW speed and density and

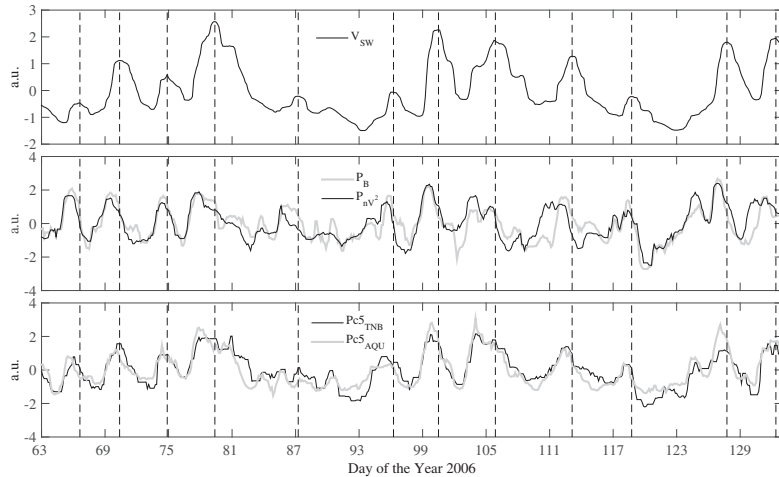


Fig. 4. – The SW and geomagnetic time series from March to May 2006. Top panel: The SW speed. Middle panel: The power in the Pc5 frequency range of the IMF strength (gray) and SW dynamic pressure (black). Bottom panel: The Pc5 power at TNB (black) and AQU (gray), obtained from the sum of the power on the H (northward) and D (eastward) horizontal components, $P = P_H + P_D$. The time series have been converted to zero mean and unitary variance. The most relevant SW speed peaks are indicated by vertical dashed lines. Figure redrawn from [19].

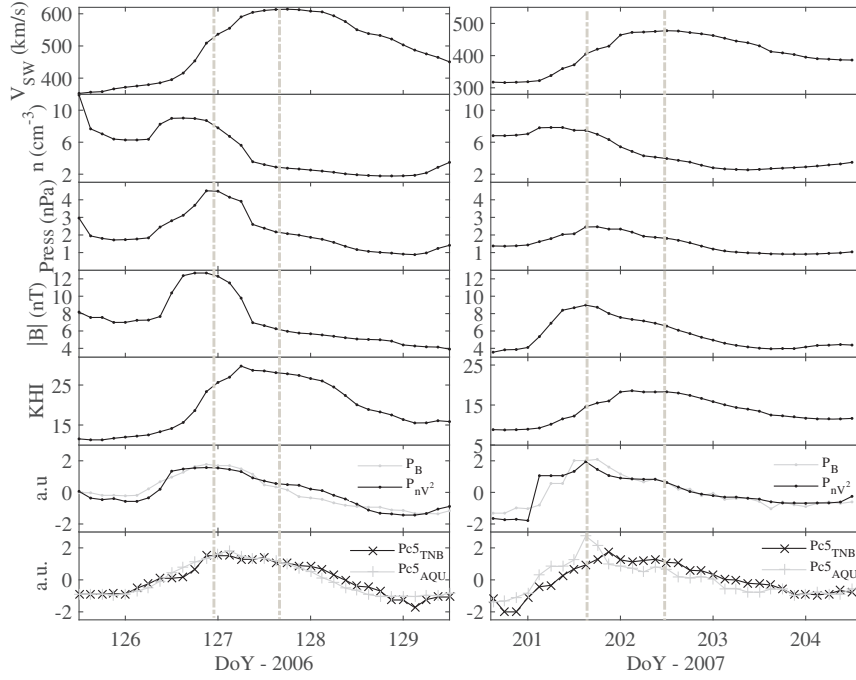


Fig. 5. – From top to bottom: the SW speed V_{SW} , particle number density n , dynamic pressure nV^2 , IMF strength B , KHI parameter, the Pc5 power of the IMF strength (gray) and SW dynamic pressure (black), TNB (black) and AQU (gray) power. The Pc5 power time series have been converted to zero mean and unitary variance. Figure redrawn from [19].

a constant IMF, a KHI parameter has been computed from the instability condition, to understand if theoretically the KHI has a role in the excitation of Pc5 power on the ground.

Figure 5 shows two events (from [19]), occurring during 2006 and 2007. In both cases the KHI parameter (obtained following the procedure indicated in [18]) attains maximum values between maximum values of V_{SW} and of SW particle density n . The KHI parameter peaks follow those observed in the ULF activity index (P) for both ground and interplanetary observations. The largest values of the KHI parameter occur when V_{SW} is still rising and follow the peak of P_{TNB} and P_{AQU} with a time delay of few hours. It is worth noting that the pulsation power at TNB persists high, longer than at AQU and in the SW and IMF fluctuations; this feature corresponds to persisting high values of the KHI parameter.

This simulation shows that the KHI is not the primary cause of the geomagnetic ULF activity in the Pc5 band, which rather seems to be due to the direct transfer of compressional waves into the magnetosphere; however, at TNB, the KHI seems to amplify the fluctuations during the whole SW high-speed period.

The experimental evidence of the dynamic response of the outer radiation belt with ULF waves generated in the CIR, is showed by [19], comparing the Pc5 power P of geomagnetic fluctuations with the relativistic electron flux observed at geosynchronous orbit by GOES 10 and 11 satellites. The results are shown in fig. 6. Recurrent, almost simultaneous enhancements of the electron flux and Pc5 power characterize the years

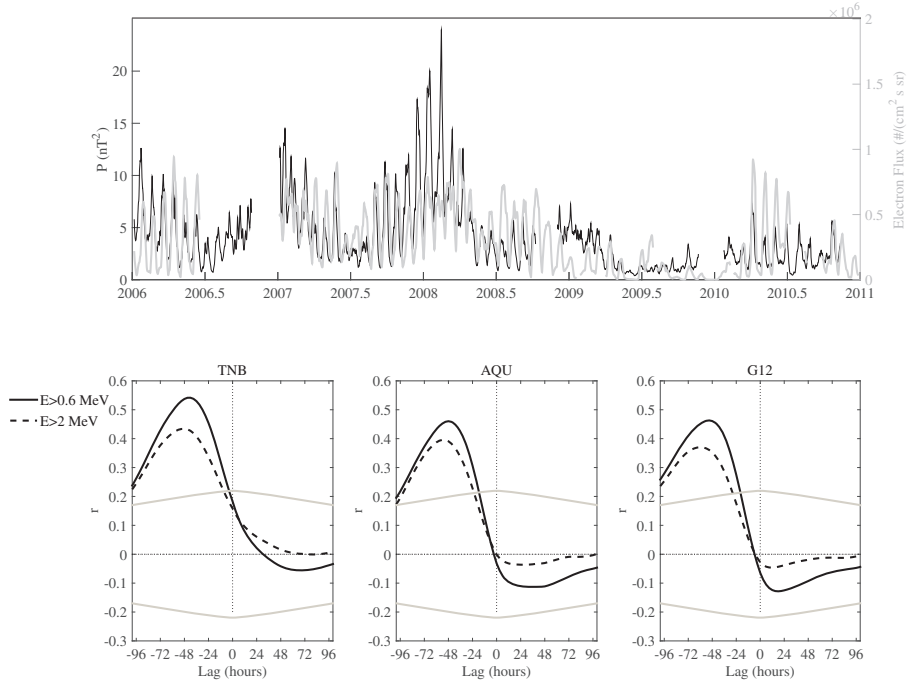


Fig. 6. – The relativistic electron flux and the Pc5 power. Top: The relativistic electron flux (> 600 keV) at geosynchronous orbit (gray) and the geomagnetic power at TNB (black). Bottom: The cross-correlation of the $E > 600$ keV (solid) and $E > 2$ MeV (dashed) electron flux with the Pc5 power at TNB (left), AQU (middle), and GOES 12 (right) during 2007 to 2008, together with the 95% confidence levels (solid gray lines). Figure redrawn from [19].

2006 to 2008 and 2010, in correspondence to the occurrence of SW streams; they tend to disappear during 2009, at the solar-cycle minimum, when the average values of the flux and power strongly decrease, often becoming negligible. In the bottom panels of fig. 6, the results of the cross-correlation analysis between the geosynchronous > 600 keV and > 2 MeV electron flux and the Pc5 fluctuation power at AQU, TNB, and GOES 12 are shown; the analysis was restricted to the interval 2007 to 2008, during which the electron flux data coverage is almost continuous and the values are significantly high. The overall result is that, in both the energy ranges, the electron flux is well correlated with the Pc5 power at the three sites, more strongly at TNB, with the maximum correlation at a time delay of approximately 2 days. In more detail, the results show also a dependence on the energy; in particular, the electrons with energy > 600 keV are more correlated and at a shorter time delay (1.8 to 2 days) with respect to the > 2 MeV electrons (2 to 2.4 days), with an approximately 9 h difference.

4. – Summary

A strong correlation is observed between the IMF and SW pressure fluctuation power and the Pc5 pulsation power, slightly time delayed. Such result indicates an almost instantaneous response of the magnetosphere to the IMF and SW pressure fluctuations, generated in the CIRs, confirming their primary role in generating Pc5 pulsations.

Some difference is observed, however, between GOES 12, AQU and TNB observa-

tions. While at geosynchronous orbit and at low latitude, the correlation with the IMF and SW pressure fluctuations is predominant; at TNB the solar-wind speed is also important. These features indicate that, with respect to the inner magnetosphere, the KHI is important on the geomagnetic field lines at the boundary of the magnetosphere, where it keeps the pulsation power level high as long as the SW speed remains high.

The energization of radiation belt electrons through the interaction with Pc5 fluctuations is demonstrated by the clear correlation of the energetic electron flux at geosynchronous orbit with the Pc5 power in the magnetosphere and at high and low latitude, at a time delay of approximately 2 days [12, 20, 13, 14, 21].

The lower correlation peak and longer time delay observed for higher-energy electrons [22, 23], indicates an energy-dependent time delay, with the > 2 MeV electron enhancement somewhat time-delayed relative to the > 600 keV electron enhancement, probably due to the time scales of the acceleration processes.

* * *

This research activity in Antarctica is supported by the Italian PNRA (Programma Nazionale di Ricerche in Antartide, PdR2013/B2.09). The author thanks P. Francia and M. De Lauretis, at the University of L'Aquila (Italy), for their comments.

REFERENCES

- [1] ALFVÉN H., *Tellus*, **9** (1957) 92.
- [2] ALFVÉN H., *Nature*, **150** (1942) 405.
- [3] KIVELSON M. G. and RUSSELL C. T., *Introduction to space physics* (Cambridge University Press) 1995.
- [4] VAN ALLEN J. A., *Energetic Particles in the Earth's External Magnetic Field*, in *Discovery of the Magnetosphere*, edited by STEWART GILLMOR C. and SPREITER J. R., *History of Geophysics*, Vol. **7** (American Geophysical Union, Washington DC) 1997, pp. 235–251.
- [5] ROEDERER J. G., *Dynamics of geomagnetically trapped radiation* (Springer-Verlag, New York) 1970.
- [6] SCHULZ M. and LANZEROTTI L. J., *Particle diffusion in the radiation belts*, in *Physics and Chemistry in Space*, Vol. **7** (Springer-Verlag, New York) 1974.
- [7] TASCIONE T. F., *Introduction to the space environment* (Krieger Publishing Company, Malabar FL) 1988.
- [8] ELKINGTON S. R., HUDSON M. K., WILTBERGER M. J. and LYON J. G., *J. Atmos. Sol. Terr. Phys.*, **64** (2002) 607.
- [9] MENK F. W., *The dynamic magnetosphere* (Springer) 2011, chapter “Magnetospheric ULF waves: a review”.
- [10] HUGHES W. J., *Magnetospheric ULF waves: a tutorial with historical perspective*, in *Solar wind sources of magnetospheric ultra-low frequency waves*, edited by ENGBRETSON M. J., TAKAHASHI K. and SCHOLER M., *AGU Geophys. Mon.*, Vol. **81** (American Geophysical Union, Washington DC) 1994, p. 1.
- [11] HUNDHAUSEN A. J., *Coronal Expansion and Solar Wind Physics and Chemistry in Space*, Vol. **5** (Springer-Verlag, Berlin, Heidelberg, New York) 1972.
- [12] ROSTOKER G., SKONE S. and BAKER D. N., *Geophys. Res. Lett.*, **25** (1998) 3701.
- [13] MATHIE R. A. and MANN I. R., *J. Geophys. Res.*, **106** (2001) 29783.
- [14] MANN I., O'BRIEN T. and MILLING D., *J. Atmos. Sol. Terr. Phys.*, **66** (2004) 187.
- [15] ELKINGTON S. R., *A Review of ULF Interactions with Radiation Belt Electrons* (American Geophysical Union) 2013 pp. 177–193. URL <http://dx.doi.org/10.1029/169GM12>.
- [16] MILLAN R. M. and BAKER D. N., *Space Sci. Rev.*, **173** (2012) 103.
- [17] GIBSON S., KOZYRA J., DE TOMA G., EMERY B., ONSAGER T. and THOMPSON B., *J. Geophys. Res.: Space Phys. (1978–2012)*, **114** (2009) A09105.

- [18] ENGBRETSON M., GLASSMEIER K.-H., STELLMACHER M., HUGHES W. J. and LHR H., *J. Geophys. Res.*, **103** (1998) 26271.
- [19] REGI M., DE LAURETIS M. and FRANCA P., *Earth Planets Space*, **67** (2015) 9.
- [20] BAKER D. N., PULKKINEN T. I., LI X., KANEKAL S. G., BLAKE J. B., SELESNICK R. S., HENDERSON M. G., REEVES G. D., SPENCE H. E. and ROSTOKER G., *J. Geophys. Res.*, **103** (1998) 17279.
- [21] KOZYREVA O., PILIPENKO V., ENGBRETSON M., YUMOTO K., WATERMANN J. and ROMANOVA N., *Planet. Space Sci.*, **55** (2007) 755.
- [22] HUDSON M. K., ELKINGTON S. R., LYON J. G., GOODRICH C. C. and ROSENBERG T. J., *Simulation of Radiation Belt Dynamics Driven by Solar Wind Variations* (American Geophysical Union) 2013 pp. 171–182. URL <http://dx.doi.org/10.1029/GM109p0171>.
- [23] RODGER C. J., CLIVERD M. A., GREEN J. C. and LAM M. M., *J. Geophys. Res.: Space Phys. (1978–2012)*, **115** (2010) A04202.